Nano Materials Science 7 (2025) 90–104

Contents lists available at ScienceDirect

Nano Materials Science

journal homepage: www.keaipublishing.com/cn/journals/nano-materials-science/

Environmentally friendly tailor-made oleo-dispersions of electrospun cellulose acetate propionate nanostructures in castor oil for lubricant applications

M.A. Martín-Alfonso [a], J.F. Rubio-Valle [a], J.P. Hinestroza [b], J.E. Martín-Alfonso [a,*], J.M. Franco [a]

[a] Chemical Product and Process Technology Research Center (Pro²TecS), Department of Chemical Engineering and Materials Science, ETSI, University of Huelva, 21071, Huelva, Spain
[b] Department of Fiber Science and Apparel Design, Cornell University, Ithaca, NY, 14853, USA

ARTICLE INFO

Keywords:
Cleaner products
Green lubricants
Nanofibers
Rheology
Tribology

ABSTRACT

The aim of this work is to find an alternative lubricating grease formulation that can be produced from renewable and biodegradable sources with minimal risks to human health and the environment. We used a castor oil and electrospun cellulose acetate propionate (CAp) as raw materials. We hypothesized that the acetyl and propionyl groups could provide an adequate chemical compatibility with the castor oil and that the electrospun nanostructures could enable improved physical stability by creating a variety of morphologies allowing the tailoring of the rheological and tribological properties of the resulting greases. The experimental results show that the use of electrospun CAp nanostructures can indeed yield physically stable formulations, even when used at low concentrations (3 wt%). The resulting dispersions went through structural transitions due to changes in the thickener morphologies and/or concentration, as shown by oscillatory rheology, oil holding capacity, tackiness, and lubrication performance in metal–metal contact. We found that the formulations, containing smooth or porous CAp nanofibers, at 5 wt% as a thickener, possess suitable rheological and tribological properties with a performance comparable to that of traditional lithium lubricating greases.

1. Introduction

Several strategies have been developed to for the sustainable use of renewable resources in economic sectors dominated by petroleum-based raw materials [1]. These strategies aimed at a better management of natural resources, a reduction in the dependence on non-renewable resources as well as a mitigation and adaptation strategy to climate change effects [2]. The concept of circular economy is a trending topic and it possess a significant challenge for the chemical industry as it re-evaluate its traditional manufacturing practices [3,4]. Friction and wear are a major cause of energy loss associated with moving parts of every engineering system [5]. Reducing friction can help to achieve carbon neutrality in a global energy audit [6] as approximately 20% of the primary energy generated, globally every year, is used to overcome friction (~100 million TJ) [7]. Lubricants are engineering products used to reduce friction and wear, which will have a great impact under the schemes of industry 4.0 [8]. The global market for lubricants did exceed 35 million tons in 2015, with an increasing demand close to 2.1% per year with a total market value close to $90 billion US [9]. It is estimated that of the 35 million tons, 55 per cent are released into the environment [10]. Most commercial lubricants and greases contain additives such as polynuclear aromatics, zinc dialkyl dithiophosphate and tri-O-cresyl phosphate [11,12] generating toxic waste. Cleaner production practices, in terms of new formulations, is an essential for adoption in the lubricant industry. The performance of a lubricating grease is a reflection of its rheological and tribological properties, which are highly influenced by the micro and nano-structures that the thickener forms during processing. Thickener structures are usually composed of entangled fibers, polymeric chains and other types of structural arrangements [13]. In addition to efforts aimed at replacing mineral and synthetic oils with vegetable oils, there are also efforts to the selection of eco-friendly thickeners. Natural polymers such as cellulose [14], lignin [15–17], polysaccharides [18–20] or organoclays [11,21,22] have been explored as grease eco-friendly thickeners. Among them, the cellulose has showed

* Corresponding author.
E-mail address: jose.martin@diq.uhu.es (J.E. Martín-Alfonso).

https://doi.org/10.1016/j.nanoms.2024.02.003
Received 24 November 2023; Accepted 5 February 2024
Available online 19 March 2024

promising results, however, the compatibility of this natural polymer with oils often requires further chemical modifications such as epoxidation [23], methylation [24,25], ethylation [26], acylation [27] or isocyanate functionalization [28]. In some cases, even if the final formulation can be assumed to be biobased, inert and nontoxic, most of the mentioned production procedures to synthesize these thickeners for greases involve relatively complex chemical reactions that require the use of hazardous chemicals and solvents [29]. Recently, Ilyin et al. [30] and Gorbacheva et al. [31,32] have reported that unmodified cellulose, in the form of nanoparticles or microfibrils, can be an effective thickener in lubricating greases. They have also highlighted the importance of the base oil in maintaining stability of the thickener particles and preventing aggregation and sedimentation. Therefore, for unmodified cellulose, it is preferable to use polar base oils such as triethyl citrate or di(2-ethylhexyl) sebacate. Additionally, the inclusion of clays can form a percolation network with appropriate rheological properties to inhibit the aggregation and sedimentation of cellulose particles [31]. Recent works has described a new method of structuring vegetable oils using electrospun nanostructures as an alternative approach [33–35]. Our hypothesis is that the high porosity, nanometric size and high surface/-volume ratio of electrospun nanostructures may allow for the formation of a unique three-dimensional networks capable of enhancing the physical interactions of the fibers with the lubricating oil. A wide variety of natural materials can be used to obtain electrospun nanostructures, including proteins, and polysaccharides. While cellulose is the most abundant biopolymer on earth, the electrospinnability of cellulose possesses many challenges due to the limited amounts of available solvents. The hydroxyl functional groups present in the backbone of cellulose molecule enables various chemical modifications such as etherification, esterification, silylation, amidation or carbamylation [36–38]. These chemical modifications can be used to increase the solubility of cellulose derivatives in hydrophobic media. Among all the cellulose derivatives, cellulose acetate propionate (CAp) is of great interests as it is widely available at commercial scales [39]. Compared with monocellulosic esters, such as cellulose acetate, CAp has better solubility, structural stability, light and weather resistance, good levelling, high gloss retention, and good transparency [40,41]. These enhanced properties are due to the presence of acetyl and propyl groups. CAp have been explored for extensive applications in the automotive and high-end furniture paint industry [42], as well as in printing inks [43], and in the extrusion and injection molding of bioplastics [42,44,45]. We hypothesize that the presence of acetyl and propyl groups present in the chemical structure of the CAp polymer could provide adequate compatibility with a vegetable oil, and that nanostructures of electrospun CAp could be used as thickening agents to create lubricating greases with unique rheological and tribological properties. The aim of this work is to develop environmental-friendly lubricating greases based on electrospun CAp nanostructures and castor oil with similar or better rheological and tribological performance than that of a multipurpose lubricating grease. Castor oil was chosen due to the great potential as biodegradable lubrication base oil [46]. Castor oil is a vegetable oil that easily forms a protective lubricating layer on the metal friction surface [47]. Further, due to its high viscosity, castor oil is more suitable than other vegetable oils as base oil of semisolid lubricants [48], and exhibits superior lubrication performance [49]. Moreover, castor oil is highly available, cost-effective, biodegradable, ecofriendly and easy to extract from castor seeds. We aim at creating alternatives that may potentially replace current petroleum-based semisolid lubricants. To achieve this goal, the influence of physicochemical, shear and extensional rheological properties of CAp solutions on its electrospinnability was studied. A wide spectrum of nanoarchitectures, including porous structures, with potential for structuring vegetable oils were obtained. The impact of the nanostructure's morphology, surface properties and concentration on the rheological, tribological and functional properties of the resulting dispersions was also assessed.

2. Materials and methods

2.1. Materials

Commercial cellulose acetate propionate (CAp) with an average molecular weight of 75.000 g mol^{-1}, and a degree of substitution (DS) of acetyl, propionyl and hydroxyl groups of 0.21, 2.64 and 0.15 [50] was obtained from Merck Sigma-Aldrich. Dichloromethane (DM, purity ≥99.8%) and ethanol (EtOH, purity ≥99.7%) were also purchased from Merck Sigma-Aldrich and used without further purification. Castor oil (211 cSt at 40 °C, Guinama, Spain) was used as a base lubricating oil. The fatty acid composition and main physical properties of this vegetable oil can be found elsewhere [51]. A commercially available multipurpose lithium lubricating grease (NLGI grade 2) commercialized by Bellota, Spain was used as a reference.

2.2. Preparation and characterization of CAp spinning solutions

CAp was dissolved in a mixed solvent composed of DM and EtOH (DM/EtOH weight ratios between 7/3 and 10/0). All solutions were magnetically stirred at 500 rpm at room temperature (~23 °C) for 3 h to obtain homogeneous and transparent electrospinning solutions. CAp solutions were characterized via electrical conductivity, surface tension as well as shear and extensional viscosity measurements. Electrical conductivity was measured at room temperature (~23 °C) with a CE GLP31 conductivity meter from Crison (Barcelona, Spain). The conductivity cell was calibrated using standard KCl solutions. Surface tension was determined also at room temperature in a Sigma 703D tensiometer (Biolin Scientific, Beijing, China), using a 39.24 mm wide × 0.1 mm thick platinum Wilhelmy plate. At least three measurements of electrical conductivity and surface tension were obtained for each sample. The rheological properties of the CAp solutions were investigated under shear deformation using an ARES (Rheometric Scientific, UK) rheometer, and under extensional deformation using the HAAKE CaBER-1 capillary breakup rheometer (Thermo Scientific, Germany). Rotational rheometry measurements were performed at 23 °C, in a shear rate range of 1–500 s^{-1} using a Couette geometry (16 mm inner diameter and 1 mm gap width). Extensional measurements were performed at 23 °C using plates with a diameter d = 6 mm and the sample was loaded at an initial gap of 2 mm. An exponential strike time of 10 ms and a final separation of 6 mm were applied for all cases.

2.3. Electrospinning and characterization of the resulting CAp electrospun structures

CAp solutions were electrospun in a DOXA chamber from Microfluidics (Málaga, Spain). A volume of 10 mL was placed in a syringe fitted with a 19-G needle and coupled to a high-voltage power. We used a voltage of 15 kV, a feed rate of 1 ml/h and a tip-to-collector distance of 15 cm. All experiments were performed at room temperature (22 ± 1 °C) and a relative humidity of 45 ± 1%. Electrospun CAp webs were carefully removed from the collector using tweezers and a spatula. The surface morphology of the CAp fibers was characterized in a FlexSEM 1000 II microscope (Hitachi, Japan), using a secondary electron detector at an acceleration voltage of 15 kV. All specimens were coated with a layer of gold before imaging. To determine average fiber diameter (AFD), around 100–120 fibers were analyzed in the different SEM images using both FIJI ImageJ (NIH, Maryland, USA) and Origin Pro 8 (Origin Lab Corporation, Northampton, USA) software.

2.4. Preparation of CAp oleo-dispersions

CAp oleo-dispersions were prepared by blending electrospun CAp nanostructures and castor oil in an open batch reactor under gentle agitation. An IKA RW-20 mixer (Germany) with a low-shear anchor impeller geometry was used. Samples were mixed for 1 h at room

temperature (~23 °C) and a rotational speed of 60 rpm. CAp content in the blends was set to 3, 4, 5 and 6 wt%. The schematic flow diagram of the manufacturing process from the electrospinning of CAp solutions to the production of CAp oleo-dispersions is shown in Fig. 1.

2.5. Characterization of CAp oleo-dispersions

The rheological properties of CAp oleo-dispersions were analyzed at 23 °C via a controlled-stress Rheoscope rheometer from Thermo Scientific (Waltham, MA, USA), using a serrated plate parallel geometry. The plates have diameters of 20 and 35 mm and a 1 mm gap were used. Small-amplitude oscillatory shear (SAOS) measurements were performed inside the linear viscoelasticity regime, in a frequency range comprised between 10^{-2} and 10^{2} rad/s. Strain sweep tests, at a frequency of 6.28 rad/s, were first performed to determine the extension of the linear viscoelasticity range. Creep and recovery tests were performed by applying a shearing stress within the LVR for 10 min, followed by a zero-stress recovery for 10 min. The compliance modulus ($J = \gamma/\sigma$) of oleo-dispersions was recorded as a function of time. The creep-recovery percentage was measured by the following equation:

$$Recovery\ rate\ (\%) = \frac{J_{max} - J_c}{J_{max}} \times 100 \quad (1)$$

where J_{max} and J_c represent the maximum compliance modulus after creep (10 min) and the equilibrium compliance after recovery (20 min). The stickiness of the oleo-dispersions was investigated using probe tack tests. The dispersions were placed between parallel plate–plate geometries of 35 mm with a fixed gap of 0.3 mm. A debonding speed of 1 mm/s was applied, and the upper plate was moved under force control with the normal force recorded throughout the test using a load transducer. The contact between plate and dispersion was maintained for 20 min before debonding. The normal stress (σ_N), strain (ϵ) and strain rate ($d\epsilon/dt$) values were calculated according to Eqs. (2)–(4) [52,53]:

$$\sigma_N = \frac{F_N(t)}{A_0} \quad (2)$$

$$\epsilon = \frac{[d(t) - h_0]}{h_0}, \quad (3)$$

$$\frac{d\varepsilon}{dt} = \frac{V_{deb}}{h_0} \quad (4)$$

where F_N is the normal force, t is the time, A_0 is the initial contact area, d and h_0 are the plate-plate separation during the tests and at the beginning of the experiment, respectively, and V_{deb} is the debonding velocity.

The oil retention capacity of the oleo-dispersions of castor oil and CAp nanostructures was evaluated as the weight ratio of released oil after centrifugation. 2 g of an oleo-dispersion was weighed and placed inside a centrifuge tube (45 mL). The specimen was centrifuged for 10 min at 750 rpm. The amount of oiling off was quantified by measuring the weight of the remaining oleo-dispersion:

$$Oil\ loss\ (\%) = \frac{W_1 - W_2}{W_1} \times 100 \quad (5)$$

where W_1, is the mass of oleo-dispersion and, W_2 is the mass of the dispersion after removing the separated oil after centrifugation.

Tribological performance of the oleo-dispersions was investigated using a Physica MCR-501 rheometer from Anton Paar (Graz, Austria) equipped with a tribological cell. The cell consisted of a 6.35 mm diameter steel ball rotating on three 45° inclined rectangular steel plates. The evolution of the friction coefficient with rotational speed was assessed in a range of sliding velocities between 10^{-4}–10^{2} (m/s), at a temperature of 23 °C and normal loads of 20 and 40 N. The stationary friction coefficient was also obtained at 23 °C by applying a normal force of 40 N and a constant sliding velocity for 20 min. The wear scars generated on the steel plates were analyzed using a BX51 microscope (Olympus, Japan).

The morphological analysis of the nanostructures in castor oil medium was carried out by scanning electron microscopy (SEM) observations carried out in a FlexSEM 1000 II microscope (Hitachi, Japan), operating at 10 kV accelerating voltage. A small amount of each sample was immersed in n-hexane for 5 days to extract the oil. The solvent was carefully replaced 1–2 times a day until oil extraction was complete. The samples were then dried at room temperature. Finally, the samples were coated with a thin layer of gold.

Fourier transformed infrared spectroscopy (FTIR) spectra of raw materials and oleo-dispersions was obtained using a typical KBr method with a JASCO FT/IR-4200 spectrometer (JASCO, Tokyo, Japan). Each sample was scanned 46 times at a resolution of 4 cm^{-1} over the wavenumber region of 4000–400 cm^{-1}.

2.6. Statistical analysis

All of the experiments were carried out at least in two replicates. The data were recorded as means ± standard deviation and were analyzed using Origin Pro 8 software (Origin Lab Corporation, Northampton, USA).

3. Results and discussion

3.1. Physicochemical properties of the CAp solutions

The electrospinnability of a polymer depends on some physicochemical properties of the precursor solution such as surface tension, electrical conductivity and viscosity [34,54–56]. Table 1 shows the values of surface tension, electrical conductivity and dynamic viscosity of CAp solutions in a mixed solvent of DM/EtOH: 7/3. We observed that the surface tension slightly decreased with increasing concentration of CAp ranging from 23.4 mN/m for the 1 wt% sample to 13.3 mN/m for the sample having 20 wt% of CAp. This decrease in the surface tension is in

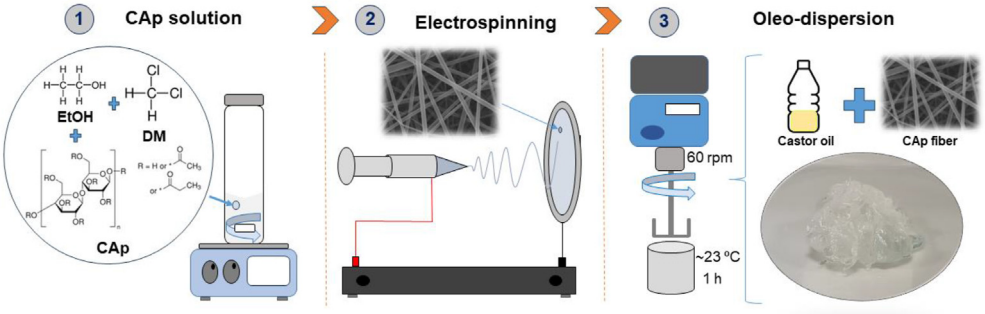

Fig. 1. Schematic flow diagram of the manufacturing process of CAp oleo-dispersions.

Table 1
Surface tension, electrical conductivity, shear viscosity (η), extensional viscosity (η_{ext}) and relaxation time (λ) values of CAp spinning solutions in DM/EtOH: 7/3.

Spinning solutions	Surface tensión, σ (mN/m)	Electrical conductivity, Λ (μS/cm)	Newtonian viscosity, η (Pa.s)	η_0 (Pa.s)	η_∞ (Pa.s)	$\dot{\gamma}_c$ (s^{-1})	p (−)	n (−)	Extensional viscosity, η_{ext} (Pa.s)	Relaxation time, λ (ms)
1 wt% CAp	23.4 ± 0.03	4.52 ± 0.09	0.0074	–	–	–	–		0.023	2.63
2 wt% CAp	23.1 ± 0.03	9.18 ± 0.11	0.0089	–	–	–	–		0.027	4.17
3 wt% CAp	22.8 ± 0.03	5.90 ± 0.10	–	0.027	0.012	52.1	5.64	0.83	0.089	22.1
5 wt% CAp	21.1 ± 0.03	4.42 ± 0.09	–	0.059	0.019	24.8	2.75	0.72	0.17	65.1
7 wt% CAp	20.2 ± 0.03	4.31 ± 0.08	–	0.175	0.028	22.8	3.19	0.65	0.52	124.9
10 wt% CAp	18.4 ± 0.02	3.74 ± 0.08	–	1.212	0.037	8.48	2.24	0.58	3.6	152.1
12.5 wt% CAp	17.2 ± 0.02	3.19 ± 0.07	–	8.69	0.064	4.30	2.16	0.53	25.3	178.3
15 wt% CAp	15.9 ± 0.02	2.56 ± 0.06	–	13.29	0.120	5.40	2.15	0.49	39.9	213.7
20 wt% CAp	13.3 ± 0.01	1.40 ± 0.05	–	79.35	0.192	4.86	2.17	0.44	247.5	297.6

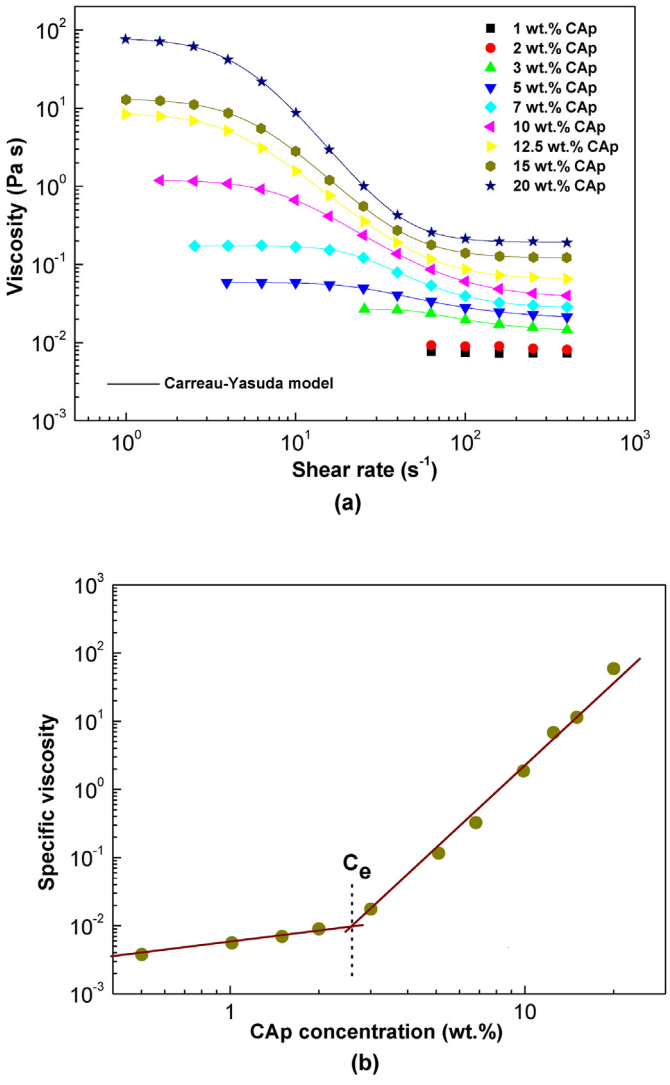

Fig. 2. (a) Viscous flow curves for CAp solutions in DM/EtOH: 7/3 as a function of concentration, and (b) plot of specific viscosity (η_{sp}) as a function of CAp concentration.

quantitative agreement with results reported by other authors [57,58]. Lower surface tension, causes an improvement of the electrospinability of the solution as electrostatic forces need to overcome the surface tension forces in order to create a Taylor cone [59].

The values of the electrical conductivity initially increased with CAp concentration for the systems prepared at 1 and 2 wt%. However, for the solutions at concentrations higher than 2%, a gradual decrease was noted. The decrease can be ascribed to a reduced polymer mobility caused by the entanglement present at higher concentrations [54].

Fig. 2a displays dynamic viscosity measurements for the CAp solutions. The specimens at 1 and 2 wt% of CAp exhibited a Newtonian behavior in all ranges of shear rate studied. However, when the CAp concentrations increased above 2 wt%, a non-Newtonian rheological response was observed. This non-Newtonian response follows a Carreu-Yasuda model ($R^2 > 0.99$).

$$\eta = \eta_\infty + \frac{(\eta_0 - \eta_\infty)}{\left[1 + \left(\frac{\dot{\gamma}}{\dot{\gamma}_c}\right)^p\right]^{\frac{1-n}{p}}} \quad (6)$$

where, η is the non-Newtonian viscosity, η_∞ and η_0 are the viscosities at infinite and zero shear rates. $\dot{\gamma}$ is the shear rate, $\dot{\gamma}_c$ is the critical shear rate for the onset of the non-Newtonian region, p is a fitting exponent and n is the flow index. Parameters for the best fit to the Carreu-Yasuda model are shown in Table 1. We noted that an increase in CAp concentration is reflected in an increase in the values of η_0, η_∞ and n, and a decrease in the values of $\dot{\gamma}_c$. This behavior is in agreement with previous results reported on spinning solutions based on chitosan [60] and polyamide-6 [61].

Fig. 2b displays the relationship between specific viscosity (η_{sp}) and CAp concentration for all solutions. This diagram allows for the determination of the critical entanglement concentration (C_e), a characteristic parameter that delimits the semi-diluted unentangled and the semi-diluted entangled regimes [34]. C_e was determined to be 2.5 wt%, the concentration at which the scaling exponent increases from $\eta_{sp} \propto C^{1.41}$ to a $\eta_{sp} \propto C^{6.37}$. The magnitude of the scaling exponents are in quantitative agreement with those expected for a neutral polymer in a good solvent [62,63]. C_e can be used to roughly predict the adequate electrospinnability of polymer solutions and the morphology of electrospun structures [64,65]. It has been suggested that the solution concentration should be at least 2–2.5 times C_e [64,65]. Various fiber morphologies, including beaded-fibers and uniform free bead-fibers, have been linked to different polymer concentration domains [66]. As explained below, CAp solutions with concentrations greater than 5 wt% are more likely to be appropriate for producing uniform bead-free fibers. Further, these experimental results serve as a confirmation of the decrease in electrical conductivity at values over 2 wt% concentration indicating a lower mobility of the macromolecules at higher concentrations.

Since a polymer solution undergoes elongational flow and extension during electrospinning, extensional rheology provides information that complements shear rheology measurements [67]. We evaluated the extensional properties of the CAp solutions by capillary rupture experiments. Fig. 3a displays the evolution of D_{min} (t) normalized by the initial diameter D_0 of the filament, as a function of time, for several CAp concentrations. For a 1 wt% solution, the determination of D_{min} (t) was complicated due to sudden filament breakage and lack of filament formation. However, as the CAp solution's concentration increased, the average filament diameter was found to decrease exponentially. This behavior occurs when the polymer chains are fully stretched, and the

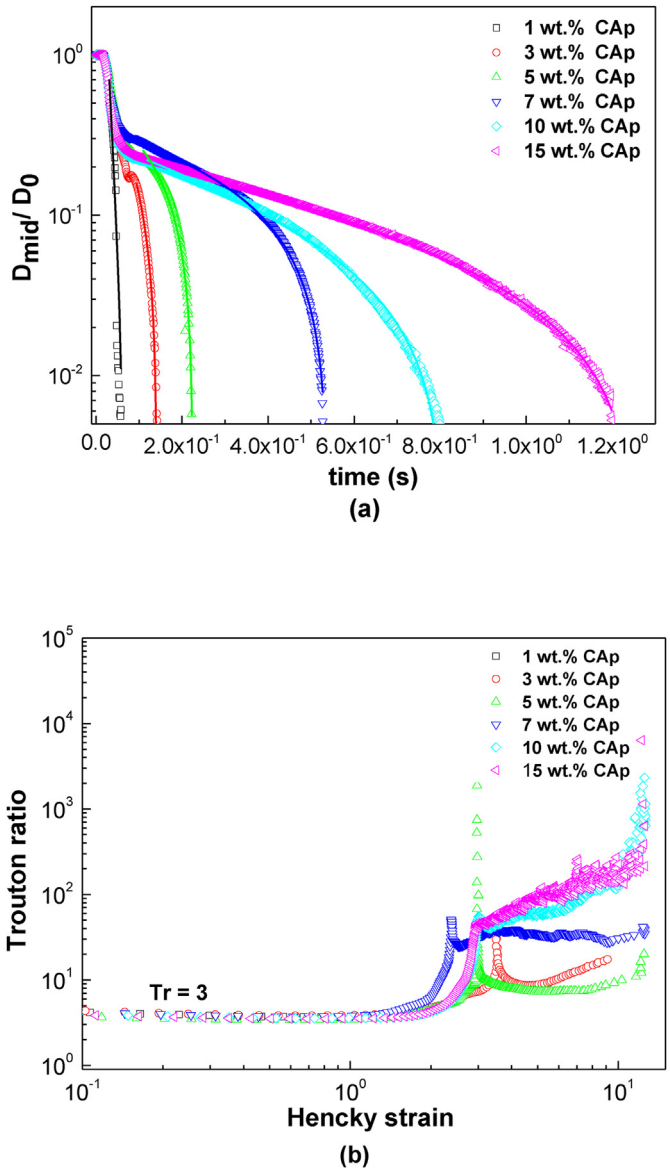

Fig. 3. a) Diameter (D_{mid}) normalized by its initial value (D_0) versus elapsed time, and (b) Trouton ratio versus Hencky strain for different polymer concentrations of CAp solutions in DM/EtOH: 7/3 tested in the CaBER rheometer.

elastic strain can no longer grow in the face of increasing capillary pressure. A functional model proposed by Anna and McKinley [68] fitted fairly well this extensional behavior ($R^2 > 0.995$):

$$\frac{D(t)}{D_0} = Ae^{-Bt} - Ct + D \tag{7}$$

In Equation (7), *A, B, C* and *D* are the fitting parameters. The value of B is related to the relaxation time (λ) of the solution ($^1/_{3\lambda}$), while the steady-state extensional viscosity is related to polymer concentration. The values of λ are tabulated in Table 1. A direct relationship between the increase in the CAp concentration and the values of λ can be observed. As the concentration of the solution increases, the relaxation time also increases, ranging from 2.63 ms for the system prepared at 1 wt% CAp to 297.6 ms for the system at 20 wt% of CAp.

The apparent extensional viscosity (η_{ext}) can be estimated from the time evolution of the filament using the following equation [69]:

$$\eta_{ext} = \frac{\sigma / D_{mid}(t)}{d\varepsilon_h(t)/dt} \tag{8}$$

where σ is the surface tension, and the Hencky strain (ε_h) is:

$$\epsilon_h = 2\ ln\left(\frac{D_0}{D_{mid}}\right) \tag{9}$$

The values of the apparent extensional viscosity are provided in Table 1. We observed that the extensional viscosity of these solutions remained reasonably constant at lower concentrations, and significantly increased with CAp concentration. This behavior is attributed to an increase in the elastic character of polymer solutions at higher concentrations [70,71].

We also studied the influence of CAp concentration on the apparent extensional viscosity values which can be expressed by the Trouton ratio (η_{ext}/η) versus the Hencky strain (ε_h) (Fig. 3b). The Trouton ratio should theoretically be 3 for Newtonian or inelastic non-Newtonian fluids [72, 73]. As it can be seen, this theoretical value was met in all cases over a wide deformation range. The Trouton ratio was found to increase significantly with time for samples at higher concentration of CAp. These results highlight the importance of performing extensional flow in addition to shear tests to evaluate the electrospinnability of polymer solutions, since shear experiments can only provide Newtonian and non-Newtonian responses, while extensional tests reveal the viscoelastic character of the solution [35,74].

3.2. *Characterization of CAp electrospun nanostructures*

Fig. 4 shows SEM micrographs of the different electrospun nanostructures obtained from CAp solutions at different concentrations. The solution prepared at 1 wt% was not able to generate fibers or interconnected particles, exhibiting a physical electrospray phenomenon, and consequently the image consists of micro-agglomerated particles (see Fig. 4a). By slightly increasing the concentration of the solution between 2 wt% and 3 wt%, morphologies with micro- and nano-sized particles connected by a thin filament (around 70–150 nm) and/or embedded in nanofiber mats were obtained (Fig. 4b-**c**). Uniform nanofiber mats were obtained from the 5 wt% solution and their diameter increased with increasing concentration, showing mean diameters of 260 ± 110 nm and 420 ± 125 nm for the systems prepared at 5 and 15 wt% (Fig. 4c–h). Further, the width of fiber diameter distribution of CAp fiber between 5 and 15 wt % CAp concentrations showed only a slight increase (see Fig. S1 in the Supporting Information).

According to Fig. 2b, the solutions with concentrations in the semi-dilute non-entangled regime produce particles or aggregates of particles, while solutions in the semi-dilute entangled regime produce fibers with high uniformity. CAp solutions at concentrations higher than 5 wt% (~2–2.5 times C_e) produced uniform fibers while solutions with concentrations around 2 wt%, which is close to the estimated C_e, mostly generated particles interconnected with fine nanofibers.

Fig. 5 shows two empirical relations between average fiber diameter and specific viscosity, as well as average fiber diameter and relaxation time of the CAp solutions. As shown in Fig. 5**a**, the average diameter and the specific viscosity exhibit an exponential relationship. It seems evident that between the non-electrospinnable and electrospinnable solutions there is a limit located between 1 and 2 wt%, as above 2 wt% concentration the molecular entanglements are sufficient to maintain a stable polymer jet.

Fig. 5b displays the average fiber diameter versus relaxation time of the CAp solutions. As can be seen, the data follows an exponential model, where a key transition value of 22 ms is observed.

We also wanted to evaluate the influence of solvent ratio on the surface and morphological properties of CAp nanostructures. For that purpose, we varied the solvent ratio of DM/EtOH. from 7/3 to 1/0. Fig. 6 contains the SEM micrographs of the electrospun nanostructures from the

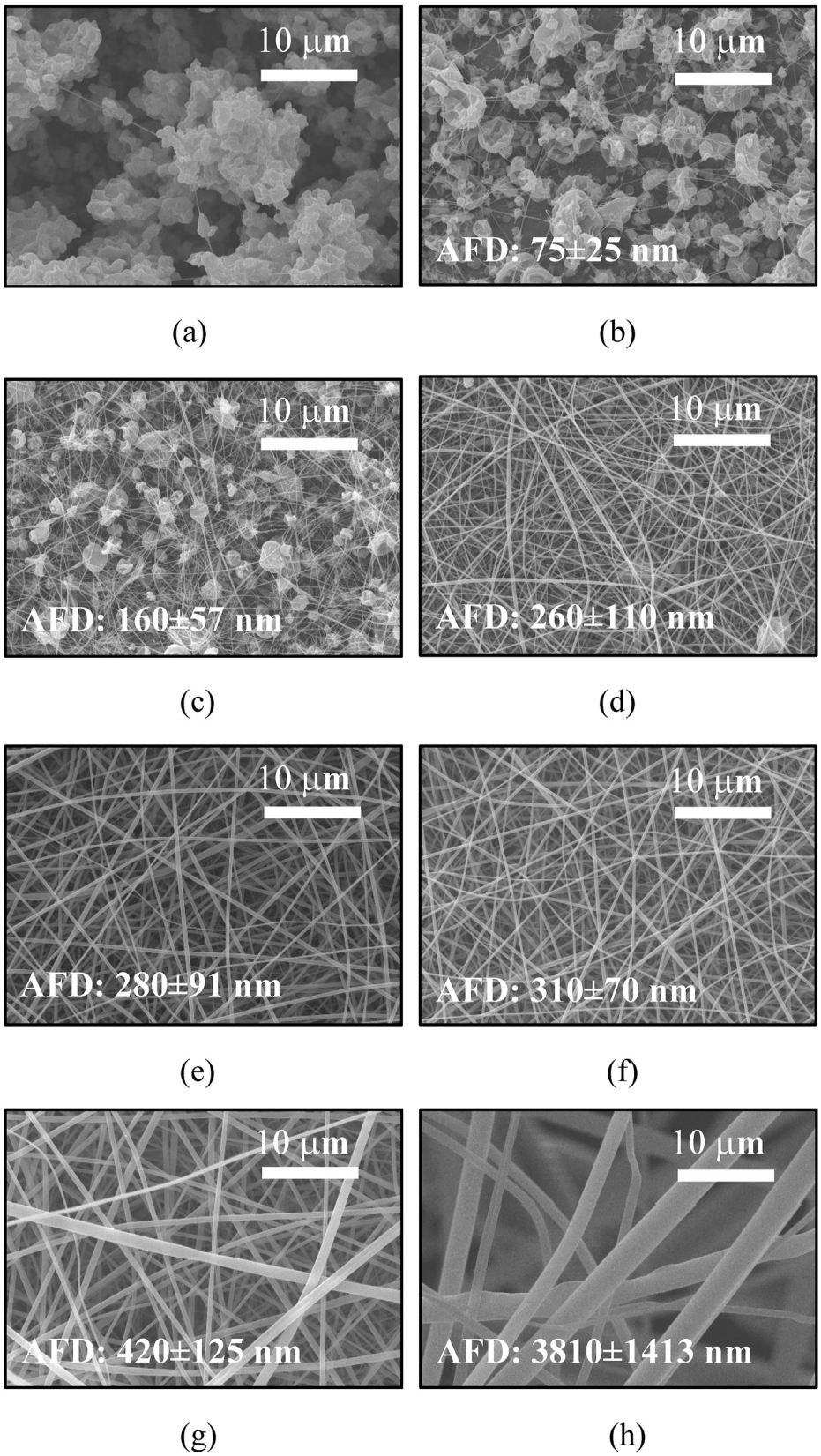

Fig. 4. SEM micrographs obtained for different concentrations of CAp solutions in DM/EtOH: 7/3: (a) 1 wt%, (b) 2 wt%, (c) 3 wt%, (d) 5 wt%, (e) 7 wt%, (f) 10 wt%, (g) 15 wt% and (h) 17 wt%.

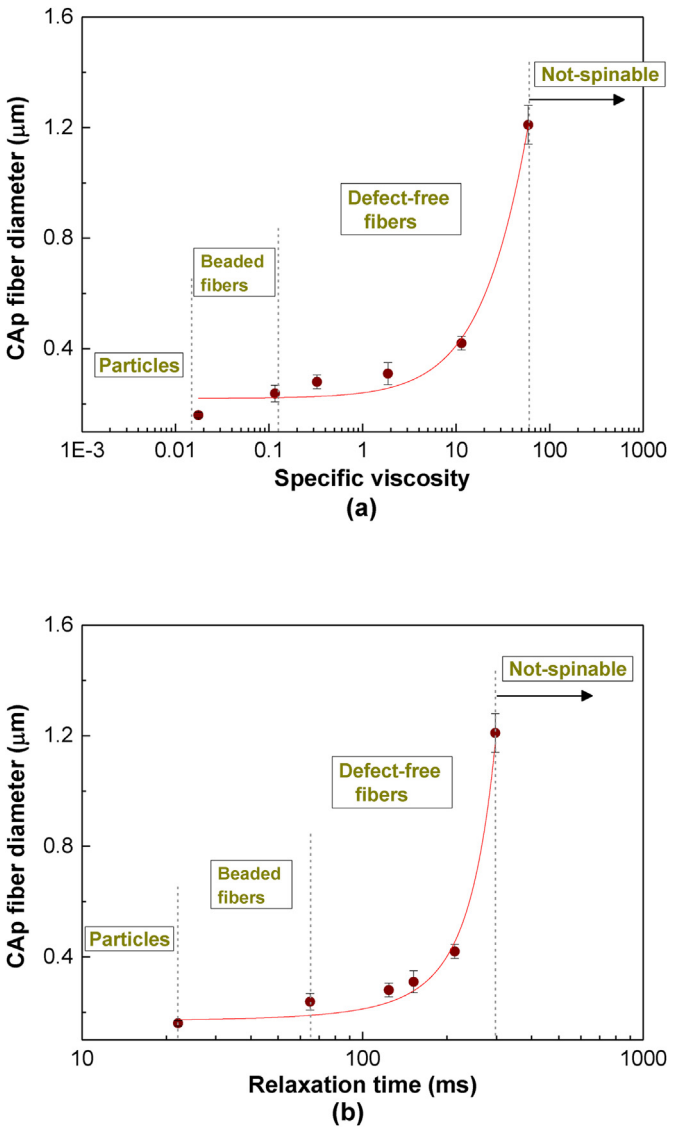

Fig. 5. Effect of a) specific viscosity and b) relaxation time of CAp solutions on the average fiber diameter of the electrospun fibers.

CAp solutions prepared at different ratios of DM/EtOH. An increase in DM content causes a significant change on the surface and morphological properties of electrospun nanostructures. Pores start appearing in the fibers, associated with morphology transitions from smooth fibers to fibers with nanoparticles, with a slight increase of AFD at 8/2 and 9/1:DM/EtOH ratios. For the samples prepared using a 10/0:DM/EtOH ratio, a porous nanostructure with a large increase in fiber diameters (see distributions in Fig. S2 of the Supporting Information) and a clear shape transition from round to flat-like fibers was observed. This behavior agrees with similar phenomena reported by several authors [34,75,76]. We believe that the formation of porous and flat/ribbon fiber structures could be attributed to the low boiling point (~39.8 °C) of DM. The rapid evaporation of the DM, on one hand, results in a large amount of heat being absorbed, as it evaporates, thereby cooling the surface of the fibers. This cooling effect causes water vapor from the humid environment to condense as droplets on the fibers surface. Upon drying, the water droplets evaporate leaving behind pores. On the other hand, the rapid release of DM generates an instability and a plasticization in the Taylor cone, resulting in a jet distortion.

3.3. Rheological, tackiness and oil loss properties of the CAp oleo-dispersions

Rheological properties of oleo-dispersions were characterized using SAOS measurements. Fig. 7a displays the evolution of storage modulus (G′) and loss modulus (G″) with frequency, and as a function of CAp concentration in a DM/EtOH: 7/3 solvent. A change in the shape of the mechanical spectra is observed when the CAp content varies. At higher CAp concentrations, the viscoelastic behavior corresponds to a so-called plateau relaxation zone. This region is characterized by having values of G′ higher than G″ over the entire frequency range, and by G″ showing a minimum and a marked increase in its frequency dependence above ~1 rad/s. This particular region has long been associated with the occurrence of physical entanglements in polymeric materials [77]. In this particular system, we believe it may be attributed to a packing effect of the entanglement network formed among the electrospun fibers. However, a different behavior was found for dispersions formulated with nanofibers obtained from spinning solution below 5 wt% CAp, as a crossover between G′ and G″ at high frequencies can be noted, which delimits the plateau and the transition zone of mechanical spectrum. This behavior suggests that a reduction in the extension of the plateau region takes place by lowering the CAp content in spinning solution. The entanglement network for this dispersion is like that created by amorphous uncrosslinked polymers of high molecular weight.

Fig. 7b displays the influence of thickener (i.e., electrospun nanofibers) concentration on the linear viscoelasticy of dispersions from solutions of CAp at 7 wt% in DM/EtOH: 7/3. All oleo-dispersions show similar mechanical spectra, corresponding to the so-called plateau relaxation zone, which is also very similar to the behavior shown by the commercially available lithium grease. We also found that an increase in thickener concentration was reflected in higher values of both G′ and G″, but not in significant changes of the loss tangent (G″/G′), indicating a progressive increase in the number of transient junction zones due to packing effects, which reduced the mobility of CAp fibers at high concentration values. Fig. 7c shows the effects of solvent ratio on the linear viscoelasticity of dispersions made with a constant concentration of thickener at 5 wt%. Interestingly, the values of the viscoelastic functions for the dispersion formulated with porous and flat/ribbon fiber structures were higher than those corresponding to the dispersion containing smooth fibers. This behavior may be associated with the formation of a more compact entanglement network due to higher interaction of castor oil and the porous nature of those fibers. However, the dispersion formulated with porous micro- and nano-particles connected by thin filaments (the one at lower concentration of CAp), showed a significant drop in the viscoelastic functions.

The dynamic viscoelastic properties of oleo-dispersions were also assessed by creep-recovery tests (Figs. 7d to f). We found that the morphologies formed by micro- and nano-sized particles connected by a few thin filaments and those with lower thickener concentrations, showed higher compliance values, indicating higher deformability. J values of the samples increased with decreasing thickener content, indicating a large degree of deformation and a smaller elasticity. The initial creep value (J_0) represents an instantaneous deformation and reflects the elastic response of the material.

The structural recovery percentage of the oleo-dispersions, indicating the recovery ability of an elastic structure after stress relief, is noted in Table 2.

As has been discussed above, when the electrospun fibers is dispersed in castor oil, the fibers arrange themselves to form a characteristic physical network depending on fiber concentration, due to the balance of forces between the colloidal fiber and the castor oil medium. Fig. 8 shows the SEM micrographs of selected electrospun nanostructures once dispersed in the oil medium, i.e. oleo-dispersions of 5 wt% CAp nanostructures obtained from solutions of 7 wt% CAp in DM/EtOH: 7/3 (a, b) and 5 wt% CAp in DM/EtOH: 9/1 (c, d), respectively. Figs. 8a and b show that the oleo-dispersion prepared with fibers has a structure like the

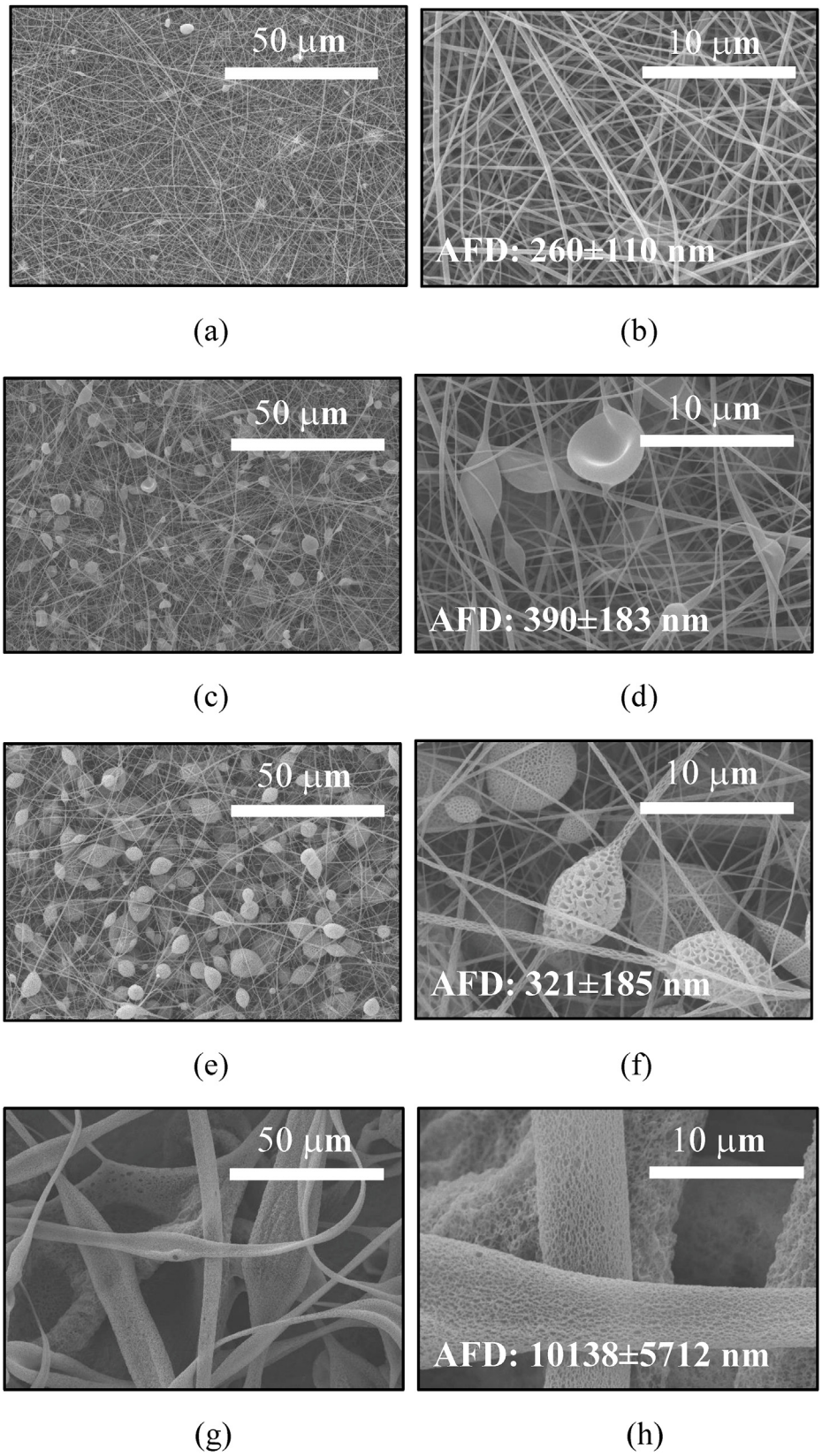

Fig. 6. SEM micrographs of structures obtained from polymer solutions containing 5 wt% CAp concentration and different ratios of DM/EtOH: (a, b) 7/3, (c, d) 8/2, (e, f) 9/1 and (g, h) 10/0.

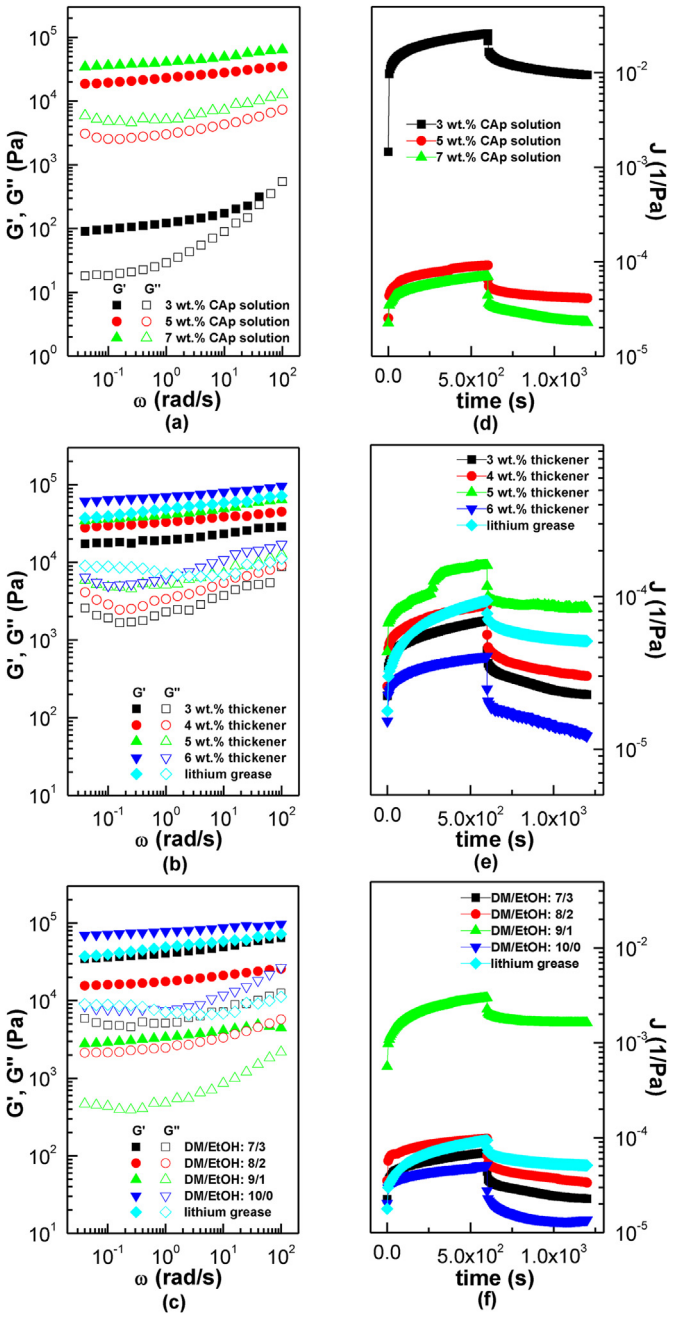

Fig. 7. Evolution of the storage and loss moduli with frequency (a, b, c), and creep-recovery curves (d, e, f) as a function of: (a, d) concentration in the spinning solution, (b, e) thickener content and (c, f) solvent ratio.

original electrospun fibers (see Fig. 4e). Interestingly, the fiber diameter was larger, probably due to swelling caused by physical diffusion phenomena. A similar effect, comparing Figs. 8c and d with Figs. 6e and f, can be observed in the nanostructure composed of fibers with nanoparticles, resulting in the occurrence of fiber-particles swelling. This degree of swelling can be estimated from the diameter fiber using the following equation:

$$Degree\ of\ swelling\ (\beta) = \frac{D_f - D_0}{D_f}$$

where D_0 refers to the average diameter of electrospun fibers and D_f to average diameters of CAp fibers in the oil medium. According to this, fiber diameter considerably increases in the percolation network, β = 65% for the nanostructure only composed of fibers and β = 82% for the bead-fiber nanostructure as a consequence of swelling. These results confirm that there is a strong physical interaction between the castor oil and the CAp electrospun nanostructure. However, there is no chemical interaction, as confirmed by the FTIR measurements (Fig. S3 in the Supporting Information).

Table 2
Rheological and tribological parameters for the oleo-dispersions studied and a reference lithium lubricating grease.

Oleo-dispersions	G°_N (Pa)	J_{max} (Pa^{-1})	% Recovery	E_{tack} (J/m^2)	Friction coefficient	Wear scar diameter (μm)
3%CAp (DM/EtOH: 70/30)-5% thickener	1.06 × 10^2	2.60 × 10^{-2}	63.6	0.72	0.074 ± 0.005	570 ± 11.3
5%CAp (DM/EtOH: 70/30)-5% thickener	2.07 × 10^4	9.18 × 10^{-5}	55.3	6.40	0.093 ± 0.006	590 ± 12.2
7%CAp (DM/EtOH: 70/30)-5% thickener	3.78 × 10^4	6.95 × 10^{-5}	67.3	6.19	0.090 ± 0.006	430 ± 10.6
7%CAp (DM/EtOH: 80/20)-5% thickener	1.68 × 10^4	9.82 × 10^{-5}	65.9	6.78	0.089 ± 0.006	530 ± 11.8
7%CAp (DM/EtOH: 90/10)-5% thickener	3.25 × 10^3	2.97 × 10^{-3}	45.4	2.91	0.081 ± 0.005	594 ± 12.4
7%CAp (DM/EtOH: 100/0)-5% thickener	1.26 × 10^4	5.14 × 10^{-5}	73.5	5.36	0.112 ± 0.009	690 ± 14.1
7%CAp (DM/EtOH: 70/30)-3% thickener	1.76 × 10^4	1.60 × 10^{-4}	47.7	3.46	0.084 ± 0.007	445 ± 11.9
7%CAp (DM/EtOH: 70/30)-4% thickener	3.05 × 10^4	8.77 × 10^{-5}	65.7	3.76	0.089 ± 0.008	438 ± 12.1
7%CAp (DM/EtOH: 70/30)-6% thickener	6.67 × 10^4	4.06 × 10^{-5}	70.0	5.35	0.099 ± 0.007	378 ± 10.9
Lithium-grease	5.46 × 10^4	9.39 × 10^{-5}	45.6	11.70	0.111 ± 0.009	521 ± 12.8
Castor oil	–	–	–	–	0.068 ± 0.005	593 ± 13.3

Although SAOS was useful to understand the linear viscoelasticity of the samples, most lubricating greases do not operate in this linear region, and under realistic conditions, at high shear rates, they undergo a process of microstructural reorganization, which eventually results in an equilibrium between the shear-induced structural degradation and a rearrangement process [78,79].

In this context, tackiness measurements could provide additional structural information about our formulations. Fig. 9 depicts the stress-strain curves for tack experiments of all oleo-dispersions prepared. According to the maximum peak stress reached during the test, the oleo-

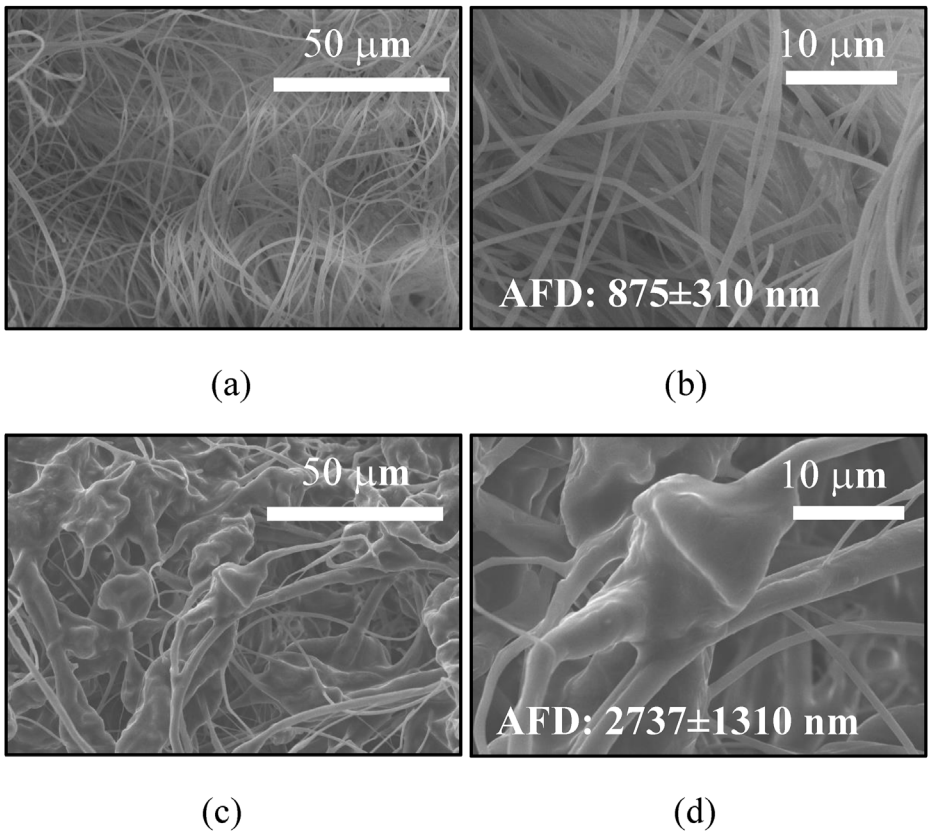

Fig. 8. SEM micrographs of nanostructures once dispersed in the oil medium at 5 wt% concentration. Nanostructures obtained from CAp solutions in DM/EtOH 7/3 at 7 wt% (a, b) and DM/EtOH: 9/1 at 5 wt% (c, d).

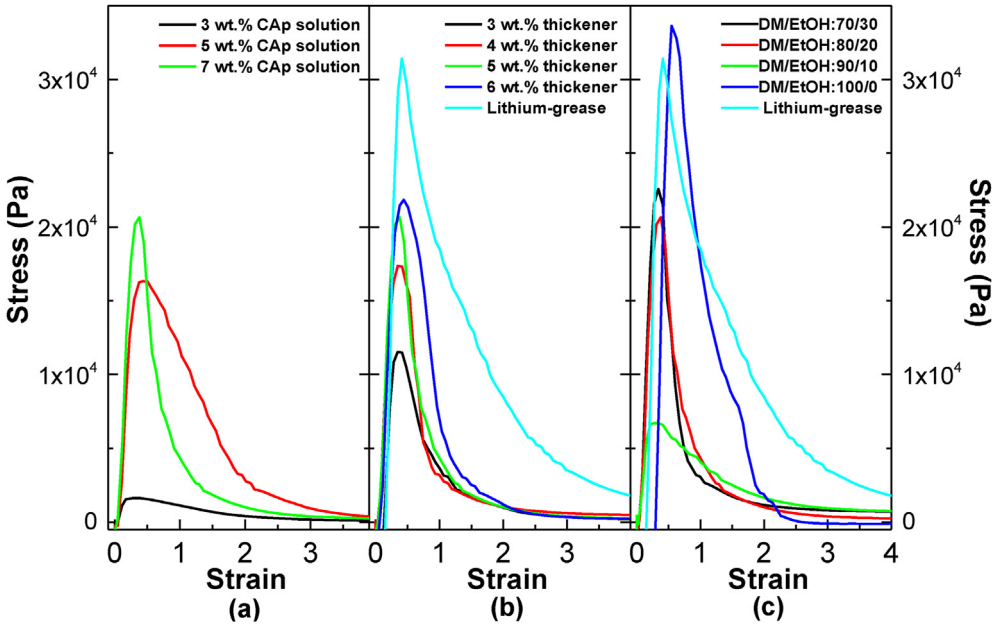

Fig. 9. Stress-strain plots in tacking tests as a function of: (a) concentration in the spinning solution, (b) thickener concentration and (c) solvent ratio (DM/EtOH).

dispersions showed an increase in tackiness when there was an increase in the concentration of the spinning solution and in the concentration of the thickener. Interestingly, the tackiness found in the oleo-dispersion formulated with porous flat/ribbon fiber structures was much higher than the values obtained for the oleo-dispersion containing smooth nanofibers. This behavior is explicitly reflected in the evolution of tackiness energy, E_{tack}, (see Table 2), which is defined per unit area as [52]:

$$E_{tack} = h_o \int_0^{\epsilon_{max}} \sigma(\epsilon) d\epsilon \tag{10}$$

It is obvious to us, that the entanglement network of the oleo-

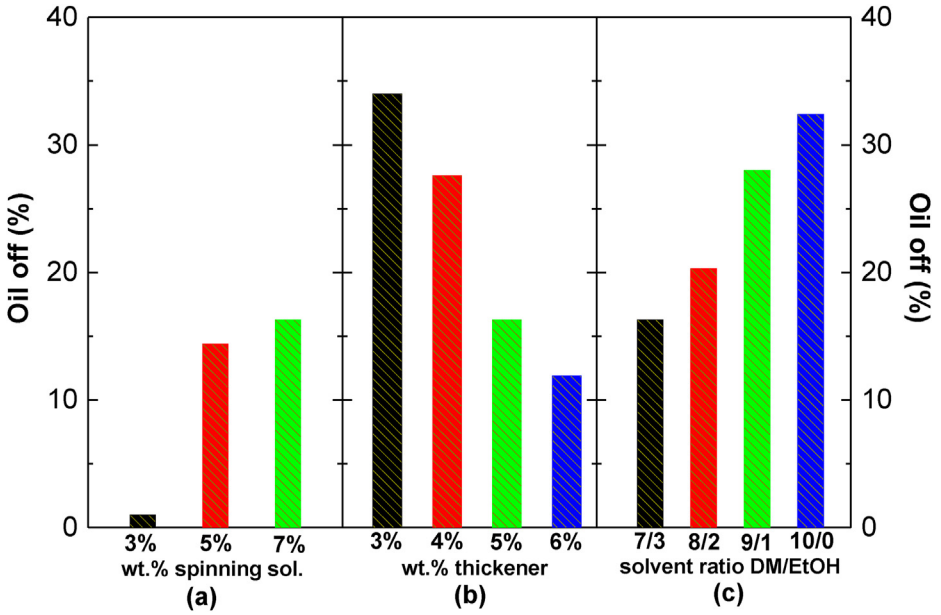

Fig. 10. Oil loss percentage as a function of: (a) concentration in the spinning solution, (b) thickener concentration and (c) solvent ratio (DM/EtOH).

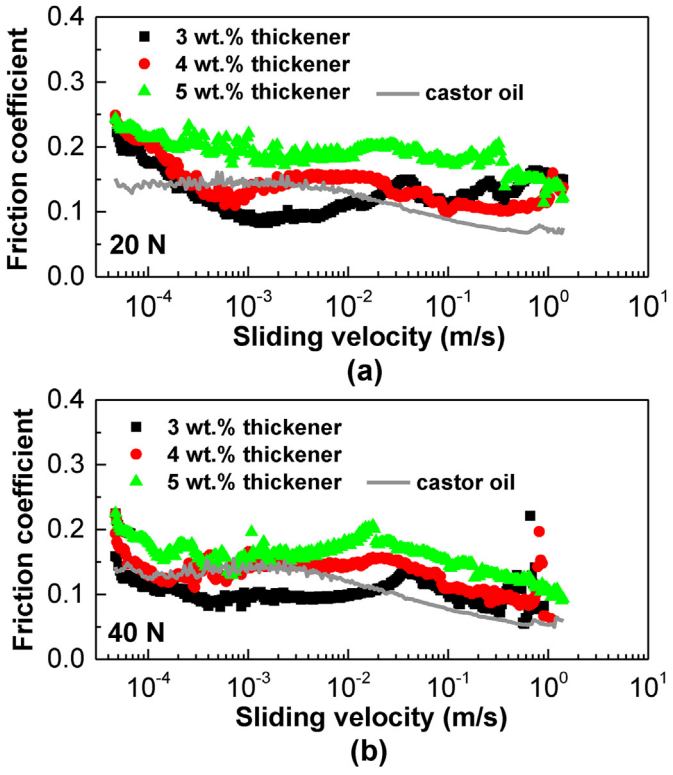

Fig. 11. Friction coefficient versus sliding velocity curves, at 23 °C, for oleo-dispersions as a function of thickener concentration at 20 N (a) and 40 N (b).

dispersions plays a key role in controlling the extensional deformation and tackiness. This can be explained by taking into account that the oleo-dispersions formulated with micro- and nano-sized particles connected by a thin filament morphologies and at lower concentrations of thickener, need less force to debond the contact and are generally less elastic [80]. This behavior is confirmed by the results from our creep rheological tests.

Finally, oil loss was evaluated as an indicator of the relative oil binding and/or trapping capacity of each oleo-dispersions and the results are shown in Fig. 10. All the oleo-dispersions exhibited self-supporting gel-like network characteristics. We also observed that when the DM content increased in the solvent ratio (porous nanostructures), lower oil loss was achieved, and we attributed that behavior to a higher functional surface ratio of the resulting oleo-dispersion as seen in Fig. 10c.

3.4. Tribological properties of CAp oleo-dispersions

The tribology of the oil-dispersions was evaluated using a ball-plate (steel-steel) contact under a rotational velocity sweep. Fig. 11 shows the Stribeck curves, friction coefficient vs. sliding velocity, under normal forces of 20 and 40 N and sliding velocities ranging from 0.05 to 1400 mm/s for oleo-dispersions formulated with smooth fibers at different thickener content (3–5 wt%). The sliding velocity was estimated following equation:

$$Sliding\ velocity = {}^{1}/\sqrt{2}\ .\ r_{ball}\ .\ \omega \tag{11}$$

where, r_{ball} is the radius of the steel contact ball (6.35 mm) and ω is the angular velocity (rad/s). In general, the dispersions at all concentrations caused a reduction in the coefficient of friction in the mixed/elastohydrodynamic lubrication regime. As shown in Fig. 11, the friction coefficient along the boundary and mixed lubrication regions increased slightly at higher thickener concentrations. This behavior can be associated to an increase in thickener concentrations [35,81].

Stationary friction tests were also performed to evaluate the lubrication function of the oleo-dispersions under mixed lubrication conditions using a normal force of 40 N and a sliding velocity of 0.047 m/s. These conditions were chosen because bearings frequently operate in this mixed regime where the surfaces are not sufficiently smooth, and the load or temperature is too high. Moreover, in this regime, a part of the friction can be attributed to the grease's internal friction [82]. Fig. 12a indicates that the coefficient of friction decreases rapidly until it reaches a stationary value around 300 s, which is indicative of the formation of an in situ protective film.

Figs. 12b to e display images of the worn surface of the steel plates. The contact surfaces were damaged after the experiments, and the rounded worn surfaces show a rough trace and deep furrows along the sliding direction. This suggests that the predominant wear mechanism was abrasion. We also observed that as thickener concentration increases, there is an increase in the friction coefficient. The friction

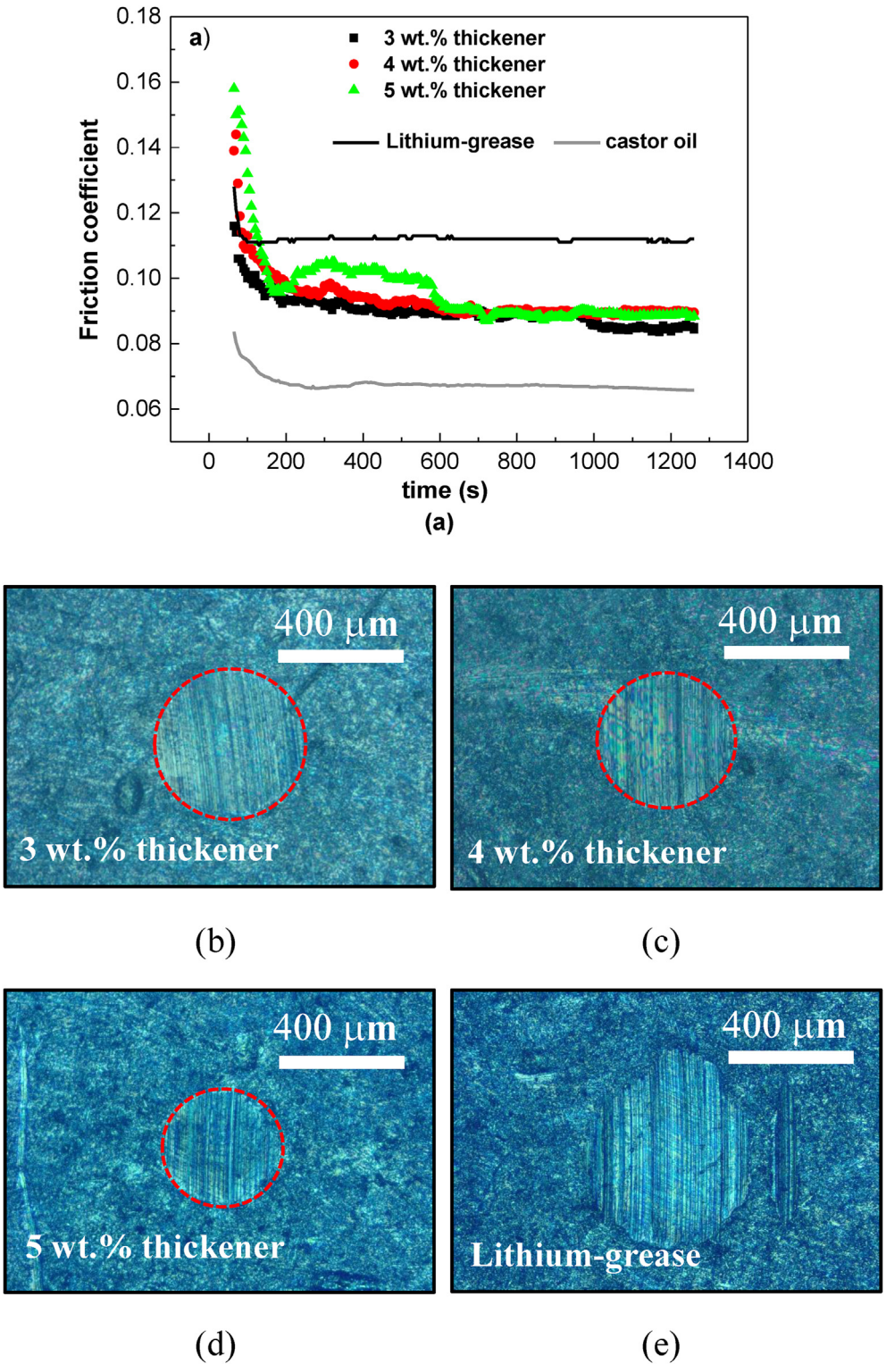

Fig. 12. (a) Friction curves for oleo-dispersions as a function of thickener concentration, (b) Optical images of the worn plate surface for steel/steel contacts.

coefficient values in grease lubricated contacts usually increase as the entrainment speed decreases, which is related to grease replenishment in the contact, as has been previously discussed by Gonçalves et al. [83–85]. Increasing the thickener concentration may reduce the contact replenishment capacity due to an increase in grease consistency while it reduces the oil bleeding ability. This is because the three-dimensional network more effectively entraps the oil [83,86], as corroborated by oil loss tests. On the other hand, the thickener's penetration into the contact increases the film thickness and must reduce the friction coefficient [85,87]. However, there is no evidence to suggest that an increase in nanostructure concentration favors thickener penetration. If penetration does occur, it does not appear to reduce friction. Previous works have reported a similar influence of thickener concentration on friction and wear when using nanosized montmorillonite [21] as a thickener in castor oil or cellulose acetate butyrate in acetyl tributyl citrate and triethyl citrate media, respectively [30,88]. More importantly, when comparing the

behavior of these oleo-dispersions with a commercial lithium grease, one can see that these new oleo-dispersions exhibit smaller friction coefficients. Further, all of the samples presented wear diameters, as shown in Figs. 12b to e and Table 2, that are comparable to those exhibited by a commercial lithium grease, or by dispersions of functionalized cellulose- or lignin [16,89].

4. Conclusions

In this work, dispersions of electrospun CAp fibers and castor oil were successfully produced and evaluated. These new formulations are potentially applicable as an environmentally friendly alternative to existing petroleum-based lubricating greases. We found that the spinnability of CAp solutions in DM/EtOH binary solvent system could be predicted based on shear/extensional properties and surface tension measurements. Uniform nanofibers were produced from CAp solutions that exhibit shear thinning behavior and a minimum relaxation time of approximately 65 ms. These requirements were achieved for CAp concentrations above 5 wt%, which is approximately 2–2.5 times the entanglement concentration, C_e. On the other hand, solutions with concentrations lower than C_e produced particles and morphologies consisting of micro- and nano-sized particles connected by thin filaments. The diameter and morphology of electrospun CAp nanostructures could be controlled by modifying the polymer concentration and the ratio of solvent in the DM/EtOH binary system. Ribbon-like CAp fibers with irregular holes were obtained on the surface of fiber electrospun using pure DM, and an exponential relationship between the relaxation time and viscosity of the spinning solution with the diameter of the resulting fiber was also found. Electrospun CAp nanostructures were able to form physically stable oleo-dispersions in castor oil, and the morphology type and surface properties (smooth and porous) of the nanostructures and their concentration played a key role to modulate their rheological and tribological properties of oleo-dispersions. The evolution of linear viscoelastic functions revealed that porous fibers and at higher concentrations have higher thickening capacity and more viscoelastic properties. This behavior is attributed to the larger fiber/oil interaction and the higher density of the fiber entanglement network. Further, these oleo dispersions have a more cohesive entanglement network, leading to an increase in tackiness. In general, the dispersion of CAp nanostructures in castor oil, employed as lubricants in a tribological contact, performs well. It reduces friction and provides wear protection similar to, or even better than, a commercial lithium lubricating grease. As a result, the produced formulations with smooth and porous CAp nanofibers at 5 wt% thickener exhibited promising rheological and tribological performance comparable to the multipurpose lithium lubricating grease classified as NLGI grade 2 according to ASTM D217.

Overall, these systems have promising rheological and tribological properties at room temperature and can be proposed as environmentally-friendly alternatives to traditional lubricating greases. However, further research is required to better understand thei tribological mechanisms involved and the viscous flow behavior at different working conditions (e.g., speed, load, and temperature).

Credit authorship contribution statement

M.A.M.A.: conceptualization, methodology, investigation, data curation, validation, formal analysis. J.F.R.V.: conceptualization, methodology, investigation, validation, formal analysis. J.P.H.: Investigation, Formal analysis, Supervision. J.E.M.A.: conceptualization, methodology, investigation, formal analysis, writing - original draft, writing - review & editing, supervision, project administration, funding acquisition. J.M.F.: conceptualization, investigation, methodology, formal analysis, validation, supervision. Analysis. All authors have given approval to the final version of the manuscript.

Data availability

Data will be made available on request.

Declaration of competing interest

The authors declare that they have no known competing financial interests or personal relationships that could have appeared to influence the work reported in this paper.

Acknowledgements

This work is part of research projects sponsored by MCIN/AEI/10.13039/501100011033 and by “ERDF A way of making Europe” (grant PID2021-125637OB-I00) and by FEDER/Junta de Andalucía Programmes (grants PY20_00751 and UHU202029). Authors gratefully acknowledge their financial support.

Appendix A. Supplementary data

Supplementary data to this article can be found online at https://doi.org/10.1016/j.nanoms.2024.02.003.

References

[1] P. Morseletto, Targets for a circular economy, Resour. Conserv. Recycl. 153 (2020) 104553, https://doi.org/10.1016/j.resconrec.2019.104553.
[2] L. Yang, X.-C. Wang, M. Dai, B. Chen, Y. Qiao, H. Deng, D. Zhang, Y. Zhang, C.M. Villas Bôas de Almeida, A.S.F. Chiu, J.J. Klemeš, Y. Wang, Shifting from fossil-based economy to bio-based economy: status quo, challenges, and prospects, Energy 228 (2021) 120533, https://doi.org/10.1016/j.energy.2021.120533.
[3] T. Keijer, V. Bakker, J.C. Slootweg, Circular chemistry to enable a circular economy, Nat. Chem. 11 (2019) 190–195, https://doi.org/10.1038/s41557-019-0226-9.
[4] S.A. Matlin, G. Mehta, H. Hopf, A. Krief, One-world chemistry and systems thinking, Nat. Chem. 8 (2016) 393–398, https://doi.org/10.1038/nchem.2498.
[5] R.V. Pawar, D.B. Hulwan, M.B. Mandale, Recent advancements in synthesis, rheological characterization, and tribological performance of vegetable oil-based lubricants enhanced with nanoparticles for sustainable lubrication, J. Clean. Prod. 378 (2022) 134454, https://doi.org/10.1016/j.jclepro.2022.134454.
[6] M. Rouhani, J. Hobley, H.-H. Ou, J.-T. Lee, S.B.S. Metla, Y.-R. Jeng, A new gateway to ecofriendly self-healing amorphous carbon tribofilms from ancient oils, Appl. Mater. Today 29 (2022) 101616, https://doi.org/10.1016/j.apmt.2022.101616.
[7] K. Holmberg, A. Erdemir, The impact of tribology on energy use and CO2 emission globally and in combustion engine and electric cars, Tribol. Int. 135 (2019) 389–396, https://doi.org/10.1016/j.triboint.2019.03.024.
[8] W.C. Satyro, C.M.V.B. de Almeida, M.J.A. Pinto Jr., J.C. Contador, B.F. Giannetti, A.F. de Lima, M.A. Fragomeni, Industry 4.0 implementation: the relevance of sustainability and the potential social impact in a developing country, J. Clean. Prod. 337 (2022) 130456, https://doi.org/10.1016/j.jclepro.2022.130456.
[9] L. Koch, A. Guntermann, K. Hirschbichler, C. Plass, T. Betke, L. Ma, T. Kilthau, H. Gröger, Sustainable tailor-made and bio-based high-performance lubricants that combine biorenewability, biodegradability and economic efficiency, Green Chem. 25 (2023) 6398–6404, https://doi.org/10.1039/D3GC00135K.
[10] A.Z. Syahir, N.W.M. Zulkifli, H.H. Masjuki, M.A. Kalam, A. Alabdulkarem, M. Gulzar, L.S. Khuong, M.H. Harith, A review on bio-based lubricants and their applications, J. Clean. Prod. 168 (2017) 997–1016, https://doi.org/10.1016/j.jclepro.2017.09.106.
[11] B. Soltannia, L. Martin-Alarcon, J. Uhryn, A. Govedarica, P. Egberts, M. Trifkovic, Enhanced rheological and tribological properties of nanoenhanced greases by tuning interparticle contacts, J. Colloid Interface Sci. 645 (2023) 560–569, https://doi.org/10.1016/j.jcis.2023.04.124.
[12] T.M. Panchal, A. Patel, D.D. Chauhan, M. Thomas, J.V. Patel, A methodological review on bio-lubricants from vegetable oil based resources, Renew. Sustain. Energy Rev. 70 (2017) 65–70, https://doi.org/10.1016/j.rser.2016.11.105.
[13] N.L.G. Guide, National Lubricating Grease Institute, 1994. Kansas City, MO, USA.
[14] N. Núñez, J.E. Martín-Alfonso, M.E. Eugenio, C. Valencia, M.J. Díaz, J.M. Franco, Influence of eucalyptus globulus kraft pulping severity on the rheological properties of gel-like cellulose pulp dispersions in castor oil, Ind. Eng. Chem. Res. (2012), https://doi.org/10.1021/ie301014v.
[15] A.M. Borrero-López, R. Martín-Sampedro, D. Ibarra, C. Valencia, M.E. Eugenio, J.M. Franco, Evaluation of lignin-enriched side-streams from different biomass conversion processes as thickeners in bio-lubricant formulations, Int. J. Biol.

Macromol. 162 (2020) 1398–1413, https://doi.org/10.1016/j.ijbiomac.2020.07.292.
[16] M. Trejo-Cáceres, M.C. Sánchez, J.E. Martín-Alfonso, Impact of acetylation process of kraft lignin in development of environment-friendly semisolid lubricants, Int. J. Biol. Macromol. 227 (2023) 673–684, https://doi.org/10.1016/j.ijbiomac.2022.12.096.
[17] Z. Wu, P.P. Thoresen, L. Matsakas, U. Rova, P. Christakopoulos, Y. Shi, Facile synthesis of lignin-Castor oil-based oleogels as green lubricating greases with excellent lubricating and antioxidation properties, ACS Sustain. Chem. Eng. 11 (2023) 12552–12561, https://doi.org/10.1021/acssuschemeng.3c01801.
[18] A. Saxena, D. Kumar, N. Tandon, Unexplored potential of acacia and guar gum to develop bio-based greases with impressive tribological performance: a possible alternative to mineral oil-based greases, Renew. Energy 200 (2022) 505–515, https://doi.org/10.1016/j.renene.2022.09.127.
[19] A. Saxena, D. Kumar, N. Tandon, Development of lubricious environmentally friendly greases using synergistic natural resources: a potential alternative to mineral oil-based greases, J. Clean. Prod. 380 (2022) 135047, https://doi.org/10.1016/j.jclepro.2022.135047.
[20] R. Sánchez, G.B. Stringari, J.M. Franco, C. Valencia, C. Gallegos, Use of chitin, chitosan and acylated derivatives as thickener agents of vegetable oils for bio-lubricant applications, Carbohydr. Polym. 85 (2011) 705–714, https://doi.org/10.1016/j.carbpol.2011.03.049.
[21] J.E. Martín-Alfonso, M.J. Martín-Alfonso, C. Valencia, M.T. Cuberes, Rheological and tribological approaches as a tool for the development of sustainable lubricating greases based on nano-montmorillonite and castor oil, Friction 9 (2021) 415–428.
[22] A. Saxena, D. Kumar, N. Tandon, Development of eco-friendly nano-greases based on vegetable oil: an exploration of the character via structure, Ind. Crops Prod. 172 (2021) 114033, https://doi.org/10.1016/j.indcrop.2021.114033.
[23] E. Cortés-Triviño, C. Valencia, M.A. Delgado, J.M. Franco, Rheology of epoxidized cellulose pulp gel-like dispersions in castor oil: influence of epoxidation degree and the epoxide chemical structure, Carbohydr. Polym. 199 (2018) 563–571, https://doi.org/10.1016/j.carbpol.2018.07.058.
[24] J.E. Martín Alfonso, R. Yañez, C. Valencia, J.M. Franco, M.J. Díaz, Optimization of the methylation conditions of kraft cellulose pulp for its use as a thickener agent in biodegradable lubricating greases, Ind. Eng. Chem. Res. 48 (2009) 6765–6771, https://doi.org/10.1021/ie9002766.
[25] N. Núñez, J.E. Martín-Alfonso, C. Valencia, M.C. Sánchez, J.M. Franco, Rheology of new green lubricating grease formulations containing cellulose pulp and its methylated derivative as thickener agents, Ind. Crops Prod. 37 (2012) 500–507, https://doi.org/10.1016/j.indcrop.2011.07.027.
[26] J.E. Martín-Alfonso, N. Núñez, C. Valencia, J.M. Franco, M.J. Díaz, Formulation of new biodegradable lubricating greases using ethylated cellulose pulp as thickener agent, J. Ind. Eng. Chem. 17 (2011) 818–823, https://doi.org/10.1016/j.jiec.2011.09.003.
[27] R. Sánchez, G. Alonso, C. Valencia, J.M. Franco, Rheological and TGA study of acylated chitosan gel-like dispersions in castor oil: influence of acyl substituent and acylation protocol, Chem. Eng. Res. Des. 100 (2015) 170–178, https://doi.org/10.1016/j.cherd.2015.05.022.
[28] R. Gallego, J.F. Arteaga, C. Valencia, M.J. Díaz, J.M. Franco, Gel-like dispersions of HMDI-cross-linked lignocellulosic materials in Castor oil: toward completely renewable lubricating grease formulations, ACS Sustain. Chem. Eng. 3 (2015) 2130–2141, https://doi.org/10.1021/acssuschemeng.5b00389.
[29] M. Guiton, D. Suárez-Montes, R. Sánchez, P. Baustert, C. Soukoulis, B.S. Okan, T. Serchi, S. Cambier, E. Benetto, Comparative Life Cycle Assessment of a microalgae-based oil metal working fluid with its petroleum-based and vegetable-based counterparts, J. Clean. Prod. 338 (2022) 130506, https://doi.org/10.1016/j.jclepro.2022.130506.
[30] S.O. Ilyin, S.N. Gorbacheva, A.Y. Yadykova, Rheology and tribology of nanocellulose-based biodegradable greases: wear and friction protection mechanisms of cellulose microfibrils, Tribol. Int. 178 (2023) 108080, https://doi.org/10.1016/j.triboint.2022.108080.
[31] S.N. Gorbacheva, Y.M. Yarmush, S.O. Ilyin, Rheology and tribology of ester-based greases with microcrystalline cellulose and organomodified montmorillonite, Tribol. Int. 148 (2020) 106318, https://doi.org/10.1016/j.triboint.2020.106318.
[32] S.N. Gorbacheva, A.Y. Yadykova, S.O. Ilyin, A novel method for producing cellulose nanoparticles and their possible application as thickeners for biodegradable low-temperature greases, Cellulose 28 (2021) 10203–10219, https://doi.org/10.1007/s10570-021-04166-1.
[33] F. Valoppi, J. Schavikin, P. Lassila, I. Laidmäe, J. Heinämäki, S. Hietala, E. Haeggström, A. Salmi, Formation and characterization of oleogels obtained via direct dispersion of ultrasound-enhanced electrospun nanofibers and cold milling, Food Struct. 37 (2023) 100338, https://doi.org/10.1016/j.foostr.2023.100338.
[34] M. Borrego, J.E. Martín-Alfonso, C. Valencia, M. del C. Sánchez Carrillo, J.M. Franco, Developing electrospun ethylcellulose nanofibrous webs: an alternative approach for structuring Castor oil, ACS Appl. Polym. Mater. 4 (2022) 7217–7227, https://doi.org/10.1021/acsapm.2c01090.
[35] J.F. Rubio-Valle, C. Valencia, M. Sánchez, J.E. Martín-Alfonso, J.M. Franco, Oil structuring properties of electrospun Kraft lignin/cellulose acetate nanofibers for lubricating applications: influence of lignin source and lignin/cellulose acetate ratio, Cellulose 30 (2023) 1553–1566, https://doi.org/10.1007/s10570-022-04963-2.
[36] S. Rodríguez-Fabià, J. Torstensen, L. Johansson, K. Syverud, Hydrophobization of lignocellulosic materials part II: chemical modification, Cellulose 29 (2022) 8957–8995, https://doi.org/10.1007/s10570-022-04824-y.
[37] W. Ge, J. Shuai, Y. Wang, Y. Zhou, X. Wang, Progress on chemical modification of cellulose in "green" solvents, Polym. Chem. 13 (2022) 359–372, https://doi.org/10.1039/D1PY00879J.
[38] K.N. Onwukamike, S. Grelier, E. Grau, H. Cramail, M.A.R. Meier, Critical review on sustainable homogeneous cellulose modification: why renewability is not enough, ACS Sustain. Chem. Eng. 7 (2019) 1826–1840, https://doi.org/10.1021/acssuschemeng.8b04990.
[39] G.W. Jeon, J.-E. An, Y.G. Jeong, High performance cellulose acetate propionate composites reinforced with exfoliated graphene, Compos. Part B Eng. 43 (2012) 3412–3418, https://doi.org/10.1016/j.compositesb.2012.01.023.
[40] K. Huang, B. Wang, Y. Cao, H. Li, J. Wang, W. Lin, C. Mu, D. Liao, Homogeneous preparation of cellulose acetate propionate (CAP) and cellulose acetate butyrate (CAB) from sugarcane bagasse cellulose in ionic liquid, J. Agric. Food Chem. 59 (2011) 5376–5381, https://doi.org/10.1021/jf104881f.
[41] J. Kujawa, E. Rynkowska, K. Fatyeyeva, K. Knozowska, A. Wolan, K. Dzieszkowski, G. Li, W. Kujawski, Preparation and characterization of cellulose acetate propionate films functionalized with reactive ionic liquids, Polymers 11 (2019) 1217, https://doi.org/10.3390/polym11071217.
[42] M. Schilling, M. Bouchard, H. Khanjian, T. Learner, A. Phenix, R. Rivenc, Application of chemical and thermal analysis methods for studying cellulose ester plastics, Acc. Chem. Res. 43 (2010) 888–896, https://doi.org/10.1021/ar1000132.
[43] T. Robert, "Green ink in all colors"—printing ink from renewable resources, Prog. Org. Coatings. 78 (2015) 287–292, https://doi.org/10.1016/j.porgcoat.2014.08.007.
[44] A.K. Mohanty, A. Wibowo, M. Misra, L.T. Drzal, Development of renewable resource-based cellulose acetate bioplastic: effect of process engineering on the performance of cellulosic plastics, Polym. Eng. Sci. 43 (2003) 1151–1161, https://doi.org/10.1002/pen.10097.
[45] D. Saloni, N. Mervine, Investigation of Bioplastics for Additive Manufacturing, 2020, pp. 365–376, https://doi.org/10.1007/978-3-030-20216-3_34.
[46] S. Asadauskas, J.H. Perez, J.L. Duda, Lubrication properties of castor oil–potential basestock for biodegradable lubricants, Tribol. Lubric. Technol. 53 (1997) 35.
[47] S. Guo, C. Li, Y. Zhang, Y. Wang, B. Li, M. Yang, X. Zhang, G. Liu, Experimental evaluation of the lubrication performance of mixtures of castor oil with other vegetable oils in MQL grinding of nickel-based alloy, J. Clean. Prod. 140 (2017) 1060–1076, https://doi.org/10.1016/j.jclepro.2016.10.073.
[48] M.C. Dwivedi, S. Sapre, Total vegetable-oil based greases prepared from castor oil, J. Synth. Lubric. 19 (2002) 229–241, https://doi.org/10.1002/jsl.3000190305.
[49] D.C. Drown, K. Harper, E. Frame, Screening vegetable oil alcohol esters as fuel lubricity enhancers, J. Am. Oil Chem. Soc. 78 (2001) 579–584, https://doi.org/10.1007/s11746-001-0307-y.
[50] R. Nilsson, H.D. Özeren, O.D. Putra, M. Hedenqvist, A. Larsson, Experimental and simulated distribution and interaction of water in cellulose esters with alkyl chain substitutions, Carbohydr. Polym. 306 (2023) 120616, https://doi.org/10.1016/j.carbpol.2023.120616.
[51] M.A. Martín-Alfonso, J.F. Rubio-Valle, J.P. Hinestroza, J.E. Martín-Alfonso, Impact of vegetable oil type on the rheological and tribological behavior of montmorillonite-based oleogels, Gels 8 (2022) 504, https://doi.org/10.3390/gels8080504.
[52] H.D. Santan, C. James, E. Fratini, I. Martínez, C. Valencia, M.C. Sánchez, J.M. Franco, Structure-property relationships in solvent free adhesives derived from castor oil, Ind. Crops Prod. 121 (2018) 90–98, https://doi.org/10.1016/j.indcrop.2018.05.012.
[53] M. Fernández, M. Landa, M.E. Muñoz, A. Santamaría, Tackiness of an electrically conducting polyurethane–nanotube nanocomposite, Int. J. Adhesion Adhes. 30 (2010) 609–614, https://doi.org/10.1016/j.ijadhadh.2010.05.011.
[54] P. Sánchez-Cid, J.F. Rubio-Valle, M. Jiménez-Rosado, V. Pérez-Puyana, A. Romero, Effect of solution properties in the development of cellulose derivative nanostructures processed via electrospinning, Polymers 14 (2022) 665, https://doi.org/10.3390/polym14040665.
[55] I. Dallmeyer, F. Ko, J.F. Kadla, Correlation of elongational fluid properties to fiber diameter in electrospinning of softwood kraft lignin solutions, Ind. Eng. Chem. Res. 53 (2014) 2697–2705, https://doi.org/10.1021/ie403724y.
[56] J.F. Rubio-Valle, M.C. Sánchez, C. Valencia, J.E. Martín-Alfonso, J.M. Franco, Electrohydrodynamic processing of PVP-doped kraft lignin micro- and nano-structures and application of electrospun nanofiber templates to produce oleogels, Polymers 13 (2021) 2206, https://doi.org/10.3390/polym13132206.
[57] S.-P. Rwei, C.-C. Huang, Electrospinning PVA solution-rheology and morphology analyses, Fibers Polym. 13 (2012) 44–50, https://doi.org/10.1007/s12221-012-0044-9.
[58] A. Bhattacharya, P. Ray, Studies on surface tension of poly(vinyl alcohol): effect of concentration, temperature, and addition of chaotropic agents, J. Appl. Polym. Sci. 93 (2004) 122–130, https://doi.org/10.1002/app.20436.
[59] A. Valizadeh, S. Mussa Farkhani, Electrospinning and electrospun nanofibres, IET Nanobiotechnol. 8 (2014) 83–92, https://doi.org/10.1049/iet-nbt.2012.0040.
[60] A. Dodero, E. Brunengo, M. Alloisio, A. Sionkowska, S. Vicini, M. Castellano, Chitosan-based electrospun membranes: effects of solution viscosity, coagulant and crosslinker, Carbohydr. Polym. 235 (2020) 115976, https://doi.org/10.1016/j.carbpol.2020.115976.
[61] M. Zoccola, A. Montarsolo, A. Aluigi, A. Varesano, C. Vineis, C. Tonin, Electrospinning of polyamide 6/modified-keratin blends, E-Polymers 7 (2007), https://doi.org/10.1515/epoly.2007.7.1.1204.
[62] L. Kong, G.R. Ziegler, Role of molecular entanglements in starch fiber formation by electrospinning, Biomacromolecules 13 (2012) 2247–2253, https://doi.org/10.1021/bm300396j.

[63] P. Gupta, C. Elkins, T.E. Long, G.L. Wilkes, Electrospinning of linear homopolymers of poly(methyl methacrylate): exploring relationships between fiber formation, viscosity, molecular weight and concentration in a good solvent, Polymer 46 (2005) 4799–4810, https://doi.org/10.1016/j.polymer.2005.04.021.
[64] S.L. Shenoy, W.D. Bates, H.L. Frisch, G.E. Wnek, Role of chain entanglements on fiber formation during electrospinning of polymer solutions: good solvent, non-specific polymer–polymer interaction limit, Polymer 46 (2005) 3372–3384, https://doi.org/10.1016/j.polymer.2005.03.011.
[65] R.R. Klossner, H.A. Queen, A.J. Coughlin, W.E. Krause, Correlation of chitosan's rheological properties and its ability to electrospin, Biomacromolecules 9 (2008) 2947–2953, https://doi.org/10.1021/bm800738u.
[66] M.G. McKee, G.L. Wilkes, R.H. Colby, T.E. Long, Correlations of solution rheology with electrospun fiber formation of linear and branched polyesters, Macromolecules 37 (2004) 1760–1767, https://doi.org/10.1021/ma035689h.
[67] M.E. Helgeson, K.N. Grammatikos, J.M. Deitzel, N.J. Wagner, Theory and kinematic measurements of the mechanics of stable electrospun polymer jets, Polymer 49 (2008) 2924–2936, https://doi.org/10.1016/j.polymer.2008.04.025.
[68] S.L. Anna, G.H. McKinley, Elasto-capillary thinning and breakup of model elastic liquids, J. Rheol. 45 (2001) 115–138, https://doi.org/10.1122/1.1332389.
[69] S. Morozova, P.W. Schmidt, A. Metaxas, F.S. Bates, T.P. Lodge, C.S. Dutcher, Extensional flow behavior of methylcellulose solutions containing fibrils, ACS Macro Lett. 7 (2018) 347–352, https://doi.org/10.1021/acsmacrolett.8b00042.
[70] M.S.N. Oliveira, R. Yeh, G.H. McKinley, Iterated stretching, extensional rheology and formation of beads-on-a-string structures in polymer solutions, J. Nonnewton. Fluid Mech. 137 (2006) 137–148, https://doi.org/10.1016/j.jnnfm.2006.01.014.
[71] S.J. Haward, V. Sharma, C.P. Butts, G.H. McKinley, S.S. Rahatekar, Shear and extensional rheology of cellulose/ionic liquid solutions, Biomacromolecules 13 (2012) 1688–1699, https://doi.org/10.1021/bm300407q.
[72] M. Negri, H.K. Ciezki, S. Schlechtriem, Spray behavior of non-Newtonian fluids: correlation between rheological measurements and droplets/threads formation, in: Prog. Propuls. Phys., EDP Sciences, Les Ulis, France, 2013, pp. 271–290, https://doi.org/10.1051/eucass/201304271.
[73] T. Sochi, Non-Newtonian flow in porous media, Polymer 51 (2010) 5007–5023, https://doi.org/10.1016/j.polymer.2010.07.047.
[74] S. Formenti, R. Castagna, R. Momentè, C. Bertarelli, F. Briatico-Vangosa, The relevance of extensional rheology on electrospinning: the polyamide/iron chloride case, Eur. Polym. J. 75 (2016) 46–55, https://doi.org/10.1016/j.eurpolymj.2015.12.003.
[75] T. Jarusuwannapoom, W. Hongrojjanawiwat, S. Jitjaicham, L. Wannatong, M. Nithitanakul, C. Pattamaprom, P. Koombhongse, R. Rangkupan, P. Supaphol, Effect of solvents on electro-spinnability of polystyrene solutions and morphological appearance of resulting electrospun polystyrene fibers, Eur. Polym. J. 41 (2005) 409–421, https://doi.org/10.1016/j.eurpolymj.2004.10.010.
[76] C.-W. Kim, D.-S. Kim, S.-Y. Kang, M. Marquez, Y.L. Joo, Structural studies of electrospun cellulose nanofibers, Polymer 47 (2006) 5097–5107, https://doi.org/10.1016/j.polymer.2006.05.033.
[77] J.D. Ferry, Viscoelastic properties of polymers. https://doi.org/10.1149/1.2428174, 1980.
[78] N. Acar, J.M. Franco, E. Kuhn, On the shear-induced structural degradation of lubricating greases and associated activation energy: an experimental rheological study, Tribol. Int. 144 (2020) 106105, https://doi.org/10.1016/j.triboint.2019.106105.
[79] M.A. Delgado, J.M. Franco, E. Kuhn, Effect of rheological behaviour of lithium greases on the friction process, Ind. Lubric. Tribol. 60 (2008) 37–45, https://doi.org/10.1108/00368790810839927.
[80] M. Harmon, B. Powell, I. Barlebo-Larsen, R. Lewis, Development of grease tackiness test, Tribol. Trans. (2019), https://doi.org/10.1080/10402004.2018.1526991.
[81] J.F. Rubio-Valle, M.C. Sánchez, C. Valencia, J.E. Martín-Alfonso, J.M. Franco, Production of lignin/cellulose acetate fiber-bead structures by electrospinning and exploration of their potential as green structuring agents for vegetable lubricating oils, Ind. Crops Prod. 188 (2022) 115579, https://doi.org/10.1016/j.indcrop.2022.115579.
[82] J.E. Martín-Alfonso, F. López-Beltrán, C. Valencia, J.M. Franco, Effect of an alkali treatment on the development of cellulose pulp-based gel-like dispersions in vegetable oil for use as lubricants, Tribol. Int. 123 (2018) 329–336, https://doi.org/10.1016/j.triboint.2018.02.027.
[83] D. Gonçalves, B. Graça, A.V. Campos, J. Seabra, J. Leckner, R. Westbroek, On the film thickness behaviour of polymer greases at low and high speeds, Tribol. Int. 90 (2015) 435–444, https://doi.org/10.1016/j.triboint.2015.05.007.
[84] D. Gonçalves, S. Pinho, B. Graça, A.V. Campos, J.H.O. Seabra, Friction torque in thrust ball bearings lubricated with polymer greases of different thickener content, Tribol. Int. 96 (2016) 87–96, https://doi.org/10.1016/j.triboint.2015.12.017.
[85] D. Gonçalves, B. Graça, A.V. Campos, J. Seabra, On the friction behaviour of polymer greases, Tribol. Int. 93 (2016) 399–410, https://doi.org/10.1016/j.triboint.2015.09.027.
[86] P. Baart, B. van der Vorst, P.M. Lugt, R.A.J. van Ostayen, Oil-bleeding model for lubricating grease based on viscous flow through a porous microstructure, Tribol. Trans. 53 (2010) 340–348, https://doi.org/10.1080/10402000903283326.
[87] H. Cen, P.M. Lugt, G. Morales-Espejel, On the film thickness of grease-lubricated contacts at low speeds, Tribol. Trans. 57 (2014) 668–678, https://doi.org/10.1080/10402004.2014.897781.
[88] S.N. Gorbacheva, A.Y. Yadykova, S.O. Ilyin, Rheological and tribological properties of low-temperature greases based on cellulose acetate butyrate gel, Carbohydr. Polym. 272 (2021) 118509, https://doi.org/10.1016/j.carbpol.2021.118509.
[89] R. Gallego, T. Cidade, R. Sánchez, C. Valencia, J.M. Franco, Tribological behaviour of novel chemically modified biopolymer-thickened lubricating greases investigated in a steel–steel rotating ball-on-three plates tribology cell, Tribol. Int. 94 (2016) 652–660, https://doi.org/10.1016/j.triboint.2015.10.028.